Journal of Analytical and Applied Pyrolysis 96 (2012) 78–85

Contents lists available at SciVerse ScienceDirect

Journal of Analytical and Applied Pyrolysis

journal homepage: www.elsevier.com/locate/jaap

Energy along Interstate I-95: Pyrolysis kinetics of Floridian cabbage palm (*Sabal palmetto*)

Li Buessing, Jillian L. Goldfarb*

Department of Chemical Engineering, University of New Hampshire, 33 Academic Way, Durham, NH 03824, United States

ARTICLE INFO

Article history:
Received 17 November 2011
Accepted 17 March 2012
Available online 31 March 2012

Keywords:
Biomass
Pyrolysis
Kinetics
Activation energy
Palm
Cabbage palm

ABSTRACT

The efficient utilization of biomass as a renewable fuel relies on the identification of readily available fuel sources and an adequate description of their decomposition reactions. Cabbage palm (*Sabal palmetto*) is one potential local energy source for the Southeastern United States. The kinetics of pyrolysis of three particle size fractions (125–250, 250–300, 300–500 μm) of cabbage palm leaf, stalk and trunk were examined using nonisothermal thermogravimetric analysis with heating rates of 25, 50 and 100 °C min^{-1} under constant nitrogen flow. Using the Arrhenius equation to calculate the activation energy and pre-exponential factor, three distinct fractions, corresponding primarily to hemicellulose, cellulose and lignin, were found to decompose over three temperature ranges, each with distinct activation energies. The largest mass loss occurred in the mid-temperature fraction (40–45%); the low temperature region had approximately 30% mass loss and the high temperature region had 15–25% mass loss. Pyrolysis at higher heating rates decreased the activation energy of each palm material, whereas particle size was not correlated with activation energy. For leaf, stalk and trunk, activation energies ranged from 64 to 115, 67 to 152 and 19 to 25 kJ mol^{-1} for the low, medium, and high temperature range fractions, corresponding to hemicellulose, cellulose and lignin, respectively.

1. Introduction

Florida has thousands of forest fires annually. Many of these are fueled by cabbage palm (*Sabal palmetto*), which typically grows to a height of 40 ft with low nutritional requirements, can tolerate a high degree of drought and salinity, and constantly loses its dried fronds. Given its widely adaptable soil environments, it is one of the most common native plants in the United States. It is a similar species to *Sabal mexicana*, which grows along the Rio Grande valley [1]. Wildfires, although often perceived as worrisome occurrences, are essential to Florida's ecosystem; burned trees become ash and water soluble nutrients that enrich the soil [2]. The Florida Forest Service maintains this natural cycle with controlled fires to prevent out-of-control wildfires. For heavily populated areas, the biomass that cannot be cycled out of the ecosystem by controlled burns could be utilized as a renewable fuel source.

Cabbage palm can grow in full sun, partial sun, or partial shade and can tolerate clay, sand, loam, alkaline, acidic, flooded and well-drained soils. Despite its hardiness, cabbage palms endure an establishment phase of between 14 and 35 years, during which time they do not exhibit an aboveground stem [3]. However, while re-establishing cabbage palms from seeds may take decades, growth from a population of trunk-less palms is considerably faster as the plot serves as a temporary reserve for rapid recovery of the palm stand [4]. Anecdotally, areas suffering wildfires along Interstate 75 in Southwestern Florida in 1999 are now flush with 10–18 ft high cabbage palm, whereas areas reduced to ash in 2007 are carpeted in a 2–4 ft high scrub of cabbage palm. From these observations and the work of McPherson and Williams [4], we deduce that the wildfires did not destroy the belowground trunks of the cabbage palm, indicating that perhaps harvesting cabbage palm at the soil surface while leaving the belowground trunk intact would increase the rate of regrowth.

In 2006 only 5% of the world's primary energy consumption came from renewable energy sources; this is projected to increase to 10% by 2030 [5]. While the potential to lower net CO_2 emissions is an attractive quality of biomass, its higher proportion of oxygen and hydrogen to carbon atoms does lower the heating value of the fuel, as breaking the C—H and C—O bonds of lignocellulosic materials releases less energy than the predominately C—C bonds of coal and other fossil fuels. However, the higher oxygen content of biomass does lead to a higher reactivity than coal and thus a lower activation energy barrier to devolatilization [6].

Pyrolysis – the thermal decomposition of a solid in the absence of oxygen – is rapidly gaining attention as a thermochemical conversion process to obtain high quality fuels from biomass. The overall process produces a mixture of gases (syngas), liquids (bio-oil) and/or solid (char), depending on the conversion mechanism

* Corresponding author. Tel.: +1 603 862 1917.
E-mail address: JillianLGoldfarb@gmail.com (J.L. Goldfarb).

0165-2370/$ – see front matter © 2012 Elsevier B.V. All rights reserved.
doi:10.1016/j.jaap.2012.03.008

used. Common approaches include rapid catalytic and noncatalytic pyrolysis and gasification [7–11]. Solid devolatilization is the first step in thermochemical conversion [12]. As a solid is devolatilized its macromolecular structure is altered because of depolymerization, vaporization, and cross-linking of the solid matrix, which leads to aromatic ring rupture, evolution of gaseous products and tars, and formation of carbonaceous char. In general, as pyrolysis temperature increases the solid product yield decreases, increasing liquid product yield until a certain temperature, at which point the gaseous product yield preferentially increases. For most biomass samples, the maximum liquid product yield occurs between about 450 and 600 °C depending on process design [7,13]. Mani et al. [14] found that bio-oil yield is the highest for the pyrolysis of straw at lower temperatures of around 450 °C with a higher gas yield at 550 °C.

For lignocellulosic biomass there exist distinct thermal events during pyrolysis corresponding roughly to the decomposition of cellulose, hemicellulose, and lignin [17]. The temperature and heating rate of pyrolysis strongly affect the quantities of each product – bio-oil, syngas, and solid char – recovered [16,17]. The development of industrial devolatilization units requires a complete understanding of the pyrolysis kinetics [18]. By using locally sourced biomass feedstocks as a renewable energy source we can reduce fuel transportation distances, decrease landfill waste and reduce pollutant burdens on groundwater and air by reducing anaerobic digestion products. Given the widespread availability of cabbage palm and the need to control its rampant growth and spread, we explore the kinetics of the pyrolysis of cabbage palm at varying particle sizes and heating rates to assist with thermochemical conversion process design for this native Floridian biomass.

2. Experimental

2.1. Materials

The cabbage palm was harvested in March 2010 from an undeveloped wooded area in a residential neighborhood of North Port, FL, USA. The tree was approximately 40 inches high from the base of the trunk in the sandy soil to the top of the fronds. Materials collected included the leaf (fronds), stalk, and trunk of the cabbage palm. The fronds were representatively sampled from each stalk, and each stalk was representatively sampled from the trunk. Likewise, the trunk was cut into rings and representatively sampled. Material was allowed to air-dry for 2 weeks before processing to reduce dampness. Each palm material was separately ground and sieved into three fractions: 125–250 μm, 250–300 μm, and 300–500 μm, and stored in glass vials awaiting kinetic analysis.

2.2. Methods

The activation energies of each palm material were determined using nonisothermal thermogravimetric analysis on a Mettler Toledo TGA/DSC 1. Between 5 and 15 mg of each sample was loaded into a clean 70 μL alumina crucible. Samples were pyrolyzed under 50 mL min^{-1} of N_2 to provide an oxygen-free environment. The method started by heating the palm material to 110 °C and holding it at 110 °C for 20 min to drive off water and purge oxygen from the system. The samples were then cooled to 25 °C under continuous nitrogen flow. The analytical step was carried out under the constant nitrogen flow between 25 °C and 600 °C and held at 600 °C for 15 min, with heating rates of 25 °C min^{-1}, 50 °C min^{-1} and 100 °C min^{-1} to query the effect of heating rate on activation energy for the three particle size fractions of each palm material. The mass of the sample was logged every second to the 10^{-6} g, along with time and temperature, accurate to 0.01 °C. Heat flow was reported as W g^{-1} by the DSC to measure overall enthalpies of pyrolysis.

TGA is often criticized for a lack of applicability to industry as it is often run at relatively slow heating rates (10–25 °C min^{-1}). As such, we query the effect of heating rate on decomposition. Many kinetic studies of biomass pyrolysis show a global reaction order of decomposition close to one [19–21]. By assuming a reaction order of one, this enables determination of the pre-exponential factor (A) and activation energy (E_a) via the Arrhenius equation of the form:

$$k = Ae^{-\frac{E_a}{RT}} \quad (1)$$

where k is the reaction rate constant, R the universal gas constant and T the absolute temperature. The decomposition rate, assuming the mass loss is a result of one or more first-order reactions, is given by Eq. (2) as:

$$\frac{dX(T)}{dT} = k * X(T) \quad (2)$$

where $X(T)$ is given by Eq. (3).

$$X(T) = \frac{m_T - m_c}{m_o} \quad (3)$$

where $X(T)$ is the difference in mass at temperature T, m_T, and the mass at complete decomposition, m_c, over the initial mass, m_o.

Given the dependence of $X(T)$ on the terminal mass, samples were held at 600 °C until the mass plateaued, ensuring complete devolatilization without mineral matter decomposition. The reaction rate constant, k, is a function of temperature; a plot of the natural log of k versus inverse temperature enables the determination of the activation energy and pre-exponential factor. For the first order reaction, the slope of this plot is equal to $-E_a/R$ and the intercept is $\ln(A)$. The activation energy and pre-exponential factor are key data used to determine the reaction mechanism for a given material. In industry, information that details the dependency of reaction rates on temperature and ramp rate is crucial to the design of efficient thermal processing units [22]. During rapid pyrolysis, the relative rates of decomposition, cracking, and condensation reactions influence the quantity, quality and long-term stability of biofuels produced [7,23].

3. Results and discussion

Each palm material (leaf, stalk, trunk) and size fraction of each material (125–250 μm, 250–300 μm, and 300–500 μm) was pyrolyzed in the TGA at the three temperature ramp rates (25, 50 and 100 °C min^{-1}) three times each to ensure reproducibility, for a total of 81 sample runs. Table 1 details the raw data for the palm trunk heated at 100 °C min^{-1} for each size fraction. (The raw data for palm trunk, stalk and leaf for all ramp rates and size fractions are available as supplemental information online in Tables S1–S8.) Fig. 1 shows the mass loss versus sample temperature of the palm trunk, 125–250 μm fraction, at the three ramp rates. The plot shows that there is little change in the percentage of mass loss across the three ramp rates, and indeed we see a very similar mass loss versus temperature profile for each ramp rate. In addition, Fig. 2 shows that the particle diameter had little effect on the rate of pyrolysis; the observed mass versus temperature data again align quite well for palm trunk pyrolyzed at 100 °C min^{-1} across the three fractions.

Biomass has three primary components: cellulose, hemicellulose and lignin. The quantity of each component will vary depending on the type of biomass, whether it is plant material such as wood chips, yard clippings, cabbage palm, or other renewable fuels such as paper waste. Most biomass sources contain approximately 30–60% cellulose, 25–35% hemicellulose and 15–30% lignin [20]. Yang et al. [24] found the decomposition of hemicellulose occurs at 220–315 °C, cellulose at 315–400 °C and lignin within a

Table 1
Raw data for palm trunk heated at 100 °C min^{-1}; standard errors reported for each activation energy data point; standard deviations reported for each average value.

		Onset T (K)	Endset T (K)	E_a (kJ mol^{-1})	A (s$^{(-1)}$)	Mass loss fraction
Low temperature mass loss regime						
Palm trunk	Trial 1	440.5	579.4	88.4 ± 2.2	7.3E+05	0.27
125–250 μm	Trial 2	448.4	578.0	88.0 ± 2.1	6.5E+05	0.27
100 °C min^{-1}	Trial 3	447.8	578.0	86.7 ± 2.0	5.0E+05	0.27
	Average	445.6 ± 4.4	578.5 ± 0.8	87.7 ± 0.9	6.3E+05 ± 1.2E+05	0.27 ± 0.003
Palm trunk	Trial 1	446.8	576.0	82.6 ± 1.8	2.3E+05	0.25
250–300 μm	Trial 2	448.4	574.7	86.0 ± 1.8	5.2E+05	0.27
100 °C min^{-1}	Trial 3	446.4	572.7	83.2 ± 1.7	2.9E+05	0.26
	Average	447.2 ± 1.1	574.5 ± 1.7	83.9 ± 1.8	3.5E+05 ± 1.5E+05	0.26 ± 0.008
Palm trunk	Trial 1	446.4	575.0	81.1 ± 1.8	1.8E+05	0.28
300–500 μm	Trial 2	444.4	572.4	82.3 ± 1.8	2.5E+05	0.28
100 °C min^{-1}	Trial 3	447.2	572.7	80.9 ± 1.9	1.7E+05	0.28
	Average	446.0 ± 1.4	573.4 ± 1.4	81.5 ± 0.8	2.0E+05 ± 4.1E+04	0.28 ± 0.004
Mid temperature mass loss regime						
Palm trunk	Trial 1	605.3	641.4	75.8 ± 1.6	3.5E+04	0.44
125–250 μm	Trial 2	606.1	645.2	76.9 ± 1.9	4.4E+04	0.45
100 °C min^{-1}	Trial 3	606.1	645.6	74.7 ± 1.0	2.9E+04	0.44
	Average	605.8 ± 0.4	644.1 ± 2.3	75.8 ± 1.1	3.6E+04 ± 7.5E+03	0.44 ± 0.005
Palm trunk	Trial 1	602.4	641.0	84.9 ± 1.3	2.4E+05	0.46
250–300 μm	Trial 2	598.8	639.8	91.0 ± 1.7	8.2E+05	0.44
100 °C min^{-1}	Trial 3	598.8	640.6	86.8 ± 1.6	3.7E+05	0.45
	Average	600.0 ± 2.1	640.5 ± 0.6	87.6 ± 3.1	4.8E+05 ± 3.0E+05	0.45 ± 0.01
Palm trunk	Trial 1	600.0	637.3	88.6 ± 1.3	5.3E+05	0.45
300–500 μm	Trial 2	597.0	637.3	86.8 ± 1.1	4.1E+05	0.41
100 °C min^{-1}	Trial 3	598.1	636.5	86.4 ± 1.4	3.7E+05	0.44
	Average	598.4 ± 1.5	637.1 ± 0.5	87.3 ± 1.2	4.4E+05 ± 8.6E+04	0.43 ± 0.02
High temperature mass loss regime						
Palm trunk	Trial 1	684.5	829.9	18.1 ± 0.3	2.5E−01	0.18
125–250 μm	Trial 2	684.5	822.0	17.8 ± 0.4	2.4E−01	0.18
100 °C min^{-1}	Trial 3	681.8	815.0	18.6 ± 0.4	2.7E−01	0.19
	Average	683.6 ± 1.5	822.3 ± 7.4	18.1 ± 0.4	2.5E−01 ± 1.7E−02	0.18 ± 0.003
Palm trunk	Trial 1	692.5	822.4	20.2 ± 0.5	3.4E−01	0.17
250–300 μm	Trial 2	697.8	818.2	21.4 ± 0.6	4.2E−01	0.19
100 °C min^{-1}	Trial 3	695.0	814.5	19.9 ± 0.5	3.3E−01	0.18
	Average	695.1 ± 2.7	818.4 ± 3.9	20.5 ± 0.8	3.6E−01 ± 4.8E−02	0.18 ± 0.009
Palm trunk	Trial 1	692.5	814.4	21.3 ± 0.6	4.1E−01	0.18
300–500 μm	Trial 2	695.0	821.9	21.8 ± 0.5	4.5E−01	0.21
100 °C min^{-1}	Trial 3	697.7	807.1	20.5 ± 0.7	3.5E−01	0.18
	Average	695.1 ± 2.6	814.5 ± 7.4	21.2 ± 0.7	4.0E−01 ± 4.6E−02	0.19 ± 0.02

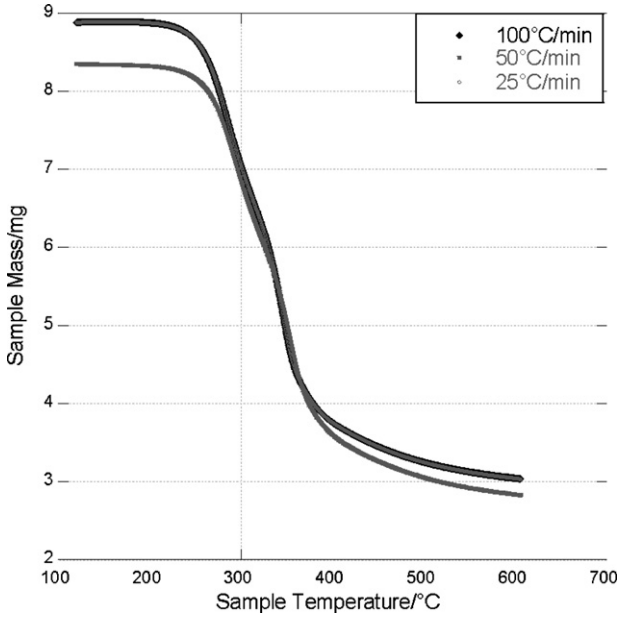

Fig. 1. Mass loss versus sample temperature for palm trunk 125–250 μm fraction heated at 25, 50 and 100 °C min^{-1}.

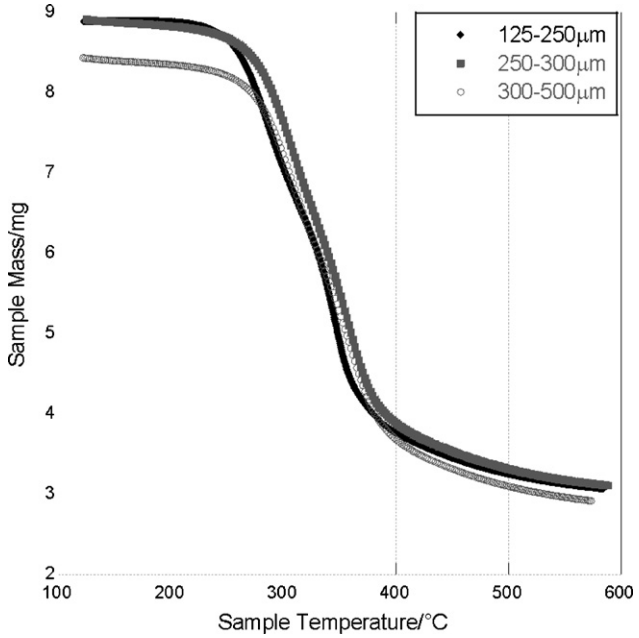

Fig. 2. Mass loss versus sample temperature for three palm trunk fractions heated at 100 °C min^{-1}.

Table 2
Global average data for palm stalk, leaf and trunk heated at 25, 50, 100 °C min^{-1} for three size fractions.

		Low temperature mass loss regime					Mid temperature mass loss regime				
		Onset T (K)	Endset T (K)	E_a (kJ mol^{-1})	A (s^{-1})	Mass loss fraction	Onset T (K)	Endset T (K)	E_a (kJ mol^{-1})	A (s^{-1})	Mass loss fraction
Palm stalk 25 °C min^{-1}	125–250 μm	448.4 ± 3.5	555.8 ± 0.8	88.9 ± 1.7	1.7E+06 ± 5.7E+05	0.30 ± 0.019	586.2 ± 1.8	619.2 ± 0.8	156.4 ± 2.4	7.4E+11 ± 3.0E+11	0.44 ± 0.021
	250–300 μm	445.2 ± 0.6	557.1 ± 0.6	88.7 ± 0.7	1.7E+06 ± 2.8E+05	0.29 ± 0.008	588.6 ± 2.4	619.1 ± 0.8	155.6 ± 1.5	5.9E+11 ± 1.8E+11	0.45 ± 0.007
	300–500 μm	444.5 ± 2.0	557.2 ± 1.7	87.8 ± 0.4	1.4E+06 ± 9.0E+04	0.30 ± 0.012	587.5 ± 1.5	619.6 ± 2.0	144.2 ± 0.2	6.0E+10 ± 3.6E+09	0.43 ± 0.018
Palm stalk 50 °C min^{-1}	125–250 μm	430.5 ± 5.4	567.6 ± 5.6	78.0 ± 0.9	1.1E+05 ± 2.8E+04	0.30 ± 0.009	593.9 ± 1.4	627.6 ± 1.4	134.9 ± 0.9	6.9E+09 ± 1.3E+09	0.44 ± 0.004
	250–300 μm	428.4 ± 2.1	565.0 ± 0.6	77.9 ± 0.1	9.5E+04 ± 4.2E+03	0.28 ± 0.013	596.4 ± 3.1	628.8 ± 0.8	137.5 ± 0.8	1.1E+10 ± 1.7E+09	0.46 ± 0.008
	300–500 μm	428.8 ± 2.0	564.5 ± 1.0	78.4 ± 0.9	1.1E+05 ± 2.1E+04	0.28 ± 0.017	596.2 ± 3.7	627.8 ± 1.4	131.2 ± 0.8	3.2E+09 ± 5.1E+08	0.45 ± 0.017
Palm stalk 100 °C min^{-1}	125–250 μm	433.5 ± 7.0	577.0 ± 1.0	78.7 ± 0.6	1.1E+05 ± 1.6E+04	0.27 ± 0.007	598.7 ± 0.6	639.7 ± 1.4	103.8 ± 1.6	1.1E+07 ± 2.9E+06	0.44 ± 0.011
	250–300 μm	439.9 ± 1.8	570.6 ± 1.5	77.7 ± 1.7	9.5E+04 ± 3.2E+04	0.29 ± 0.007	596.4 ± 2.1	637.8 ± 0.8	98.9 ± 1.4	4.8E+06 ± 9.9E+05	0.43 ± 0.012
	300–500 μm	440.9 ± 3.0	570.6 ± 2.3	83.3 ± 2.4	3.5E+05 ± 1.6E+05	0.29 ± 0.011	593.8 ± 3.1	636.1 ± 0.9	101.2 ± 2.0	7.2E+06 ± 3.4E+06	0.44 ± 0.014
Palm leaf 25 °C min^{-1}	125–250 μm	446.5 ± 2.8	555.6 ± 1.5	78.2 ± 0.3	1.4E+05 ± 1.3E+04	0.28 ± 0.003	590.0 ± 2.3	621.5 ± 2.8	140.7 ± 1.4	2.2E+10 ± 6.5E+09	0.38 ± 0.005
	250–300 μm	443.6 ± 4.8	555.1 ± 0.4	78.2 ± 0.6	1.5E+05 ± 1.9E+04	0.28 ± 0.004	589.0 ± 2.9	622.0 ± 1.8	137.3 ± 0.4	1.1E+10 ± 8.8E+08	0.40 ± 0.001
	300–500 μm	453.4 ± 2.6	554.2 ± 1.2	77.9 ± 0.9	1.3E+05 ± 2.5E+04	0.28 ± 0.002	591.7 ± 0.6	621.9 ± 0.0	126.7 ± 0.8	1.3E+09 ± 2.1E+08	0.37 ± 0.002
Palm leaf 50 °C min^{-1}	125–250 μm	428.7 ± 2.6	565.2 ± 0.2	69.6 ± 0.5	1.5E+04 ± 1.8E+03	0.26 ± 0.005	597.3 ± 1.6	631.6 ± 1.1	118.4 ± 1.2	1.9E+08 ± 4.4E+07	0.38 ± 0.005
	250–300 μm	423.7 ± 3.5	563.9 ± 1.3	69.6 ± 0.1	1.5E+04 ± 8.4E+02	0.27 ± 0.007	596.1 ± 1.7	631.7 ± 1.2	112.0 ± 2.3	6.0E+07 ± 3.1E+07	0.39 ± 0.020
	300–500 μm	428.6 ± 2.6	562.7 ± 1.2	69.4 ± 0.6	1.6E+04 ± 2.3E+03	0.27 ± 0.014	596.0 ± 0.8	630.3 ± 1.3	107.5 ± 3.8	2.7E+07 ± 2.2E+07	0.36 ± 0.006
Palm leaf 100 °C min^{-1}	125–250 μm	438.7 ± 1.7	572.3 ± 2.1	64.4 ± 0.1	4.2E+03 ± 4.3E+01	0.27 ± 0.008	592.6 ± 1.0	638.7 ± 1.7	69.2 ± 2.6	1.0E+04 ± 5.1E+03	0.40 ± 0.022
	250–300 μm	441.6 ± 1.8	571.2 ± 1.3	64.0 ± 0.6	4.0E+03 ± 4.9E+02	0.27 ± 0.009	592.4 ± 2.8	638.8 ± 2.4	68.3 ± 1.1	8.2E+03 ± 1.5E+03	0.39 ± 0.007
	300–500 μm	442.9 ± 0.5	570.6 ± 1.6	64.6 ± 1.0	4.7E+03 ± 8.3E+02	0.28 ± 0.005	594.3 ± 0.2	636.4 ± 0.8	62.6 ± 0.8	2.7E+03 ± 4.2E+02	0.37 ± 0.006
Palm trunk 25 °C min^{-1}	125–250 μm	453.3 ± 3.4	554.1 ± 2.3	114.1 ± 0.5	5.7E+08 ± 6.9E+07	0.29 ± 0.012	590.1 ± 2.1	623.1 ± 0.7	137.3 ± 2.0	1.2E+10 ± 4.7E+09	0.42 ± 0.010
	250–300 μm	461.1 ± 3.1	553.2 ± 1.8	116.2 ± 2.1	1.0E+09 ± 4.3E+08	0.27 ± 0.012	588.1 ± 2.5	622.6 ± 1.6	144.0 ± 1.3	4.7E+10 ± 1.1E+10	0.45 ± 0.007
	300–500 μm	461.8 ± 2.4	551.7 ± 1.2	117.0 ± 1.0	1.2E+09 ± 3.0E+08	0.27 ± 0.015	589.6 ± 0.0	620.1 ± 2.8	145.6 ± 0.5	7.0E+10 ± 6.5E+09	0.44 ± 0.023
Palm trunk 50 °C min^{-1}	125–250 μm	429.8 ± 5.2	564.4 ± 2.6	93.9 ± 0.4	4.2E+06 ± 4.2E+05	0.28 ± 0.006	598.3 ± 1.5	630.5 ± 1.9	115.1 ± 1.1	1.1E+08 ± 2.0E+07	0.39 ± 0.007
	250–300 μm	435.6 ± 4.3	559.1 ± 3.3	95.5 ± 1.3	5.9E+06 ± 2.1E+06	0.29 ± 0.012	597.8 ± 0.9	631.2 ± 0.8	130.4 ± 3.1	2.4E+09 ± 1.2E+09	0.46 ± 0.026
	300–500 μm	444.4 ± 4.4	560.1 ± 1.2	103.2 ± 0.9	3.6E+07 ± 8.4E+06	0.29 ± 0.002	597.1 ± 2.9	630.5 ± 1.9	127.1 ± 1.7	1.3E+09 ± 4.4E+08	0.45 ± 0.010
Palm trunk 100 °C min^{-1}	125–250 μm	445.6 ± 4.4	578.5 ± 0.8	87.7 ± 0.9	6.3E+05 ± 1.2E+05	0.27 ± 0.003	605.8 ± 0.4	644.1 ± 2.3	75.8 ± 1.1	3.6E+04 ± 7.5E+03	0.44 ± 0.005
	250–300 μm	447.2 ± 1.1	574.5 ± 1.7	83.9 ± 1.8	3.5E+05 ± 1.5E+05	0.26 ± 0.008	600.0 ± 2.1	640.5 ± 0.6	87.6 ± 3.1	4.8E+05 ± 3.0E+05	0.45 ± 0.012
	300–500 μm	446.0 ± 1.4	573.4 ± 1.4	81.5 ± 0.8	2.0E+05 ± 4.1E+04	0.28 ± 0.004	598.4 ± 1.5	637.1 ± 0.5	87.3 ± 1.2	4.4E+05 ± 8.6E+04	0.43 ± 0.019

		High temperature mass loss regime				
		Onset T (K)	Endset T (K)	E_a (kJ mol^{-1})	A (s^{-1})	Mass loss fraction
Palm stalk 25 °C min^{-1}	125–250 μm	659.3 ± 2.5	838.9 ± 5.1	21.7 ± 0.5	0.47 ± 0.034	0.17 ± 0.002
	250–300 μm	659.2 ± 3.0	828.3 ± 4.1	22.1 ± 0.4	0.50 ± 0.031	0.17 ± 0.004
	300–500 μm	665.2 ± 3.8	835.7 ± 5.8	21.8 ± 0.4	0.48 ± 0.030	0.18 ± 0.008
Palm stalk 50 °C min^{-1}	125–250 μm	677.0 ± 5.0	829.8 ± 10.5	25.8 ± 0.8	0.87 ± 0.10	0.17 ± 0.006
	250–300 μm	675.2 ± 1.6	822.2 ± 4.1	24.7 ± 0.4	0.73 ± 0.052	0.16 ± 0.006
	300–500 μm	679.3 ± 2.5	824.9 ± 4.3	24.0 ± 0.4	0.65 ± 0.039	0.16 ± 0.005
Palm stalk 100 °C min^{-1}	125–250 μm	679.6 ± 2.6	834.0 ± 1.2	26.4 ± 0.5	1.07 ± 0.28	0.19 ± 0.006
	250–300 μm	688.9 ± 4.1	824.9 ± 4.3	24.2 ± 0.3	0.66 ± 0.032	0.19 ± 0.006
	300–500 μm	697.8 ± 7.4	819.7 ± 2.3	22.6 ± 0.2	0.51 ± 0.022	0.18 ± 0.006
Palm leaf 25 °C min^{-1}	125–250 μm	665.6 ± 4.4	818.2 ± 5.5	19.2 ± 1.0	0.32 ± 0.036	0.22 ± 0.002
	250–300 μm	654.5 ± 9.0	821.7 ± 2.7	19.0 ± 0.1	0.32 ± 0.007	0.22 ± 0.003
	300–500 μm	654.3 ± 1.5	824.0 ± 2.4	19.8 ± 0.4	0.35 ± 0.021	0.22 ± 0.001
Palm leaf 50 °C min^{-1}	125–250 μm	664.2 ± 0.9	805.8 ± 5.0	20.5 ± 0.3	0.40 ± 0.020	0.15 ± 0.005
	250–300 μm	663.4 ± 2.8	818.3 ± 0.2	20.6 ± 0.4	0.41 ± 0.008	0.14 ± 0.02
	300–500 μm	663.5 ± 2.7	819.4 ± 4.3	21.2 ± 0.1	0.43 ± 0.010	0.15 ± 0.009
Palm leaf 100 °C min^{-1}	125–250 μm	669.2 ± 2.8	729.0 ± 3.1	23.4 ± 0.4	0.57 ± 0.041	0.23 ± 0.018
	250–300 μm	667.9 ± 2.2	727.4 ± 8.1	22.8 ± 0.7	0.51 ± 0.065	0.23 ± 0.002
	300–500 μm	666.1 ± 1.0	728.1 ± 7.2	23.5 ± 0.1	0.56 ± 0.017	0.24 ± 0.002
Palm trunk 25 °C min^{-1}	125–250 μm	677.7 ± 3.7	819.7 ± 8.0	16.9 ± 0.7	0.20 ± 0.024	0.19 ± 0.006
	250–300 μm	677.5 ± 1.6	832.5 ± 7.1	18.9 ± 0.2	0.28 ± 0.008	0.18 ± 0.004
	300–500 μm	671.3 ± 4.7	840.0 ± 2.8	20.4 ± 0.2	0.35 ± 0.014	0.18 ± 0.01
Palm trunk 50 °C min^{-1}	125–250 μm	686.9 ± 4.4	823.0 ± 3.4	19.7 ± 0.5	0.31 ± 0.023	0.18 ± 0.01
	250–300 μm	688.3 ± 1.3	825.7 ± 7.2	20.9 ± 0.5	0.38 ± 0.036	0.17 ± 0.006
	300–500 μm	682.5 ± 3.0	831.9 ± 4.8	21.4 ± 1.0	0.41 ± 0.061	0.17 ± 0.005
Palm trunk 100 °C min^{-1}	125–250 μm	683.6 ± 1.5	822.3 ± 7.4	18.1 ± 0.4	0.25 ± 0.017	0.18 ± 0.003
	250–300 μm	695.1 ± 2.7	818.4 ± 3.9	20.5 ± 0.8	0.36 ± 0.048	0.18 ± 0.009
	300–500 μm	695.1 ± 2.6	814.5 ± 7.4	21.2 ± 0.7	0.40 ± 0.046	0.19 ± 0.02

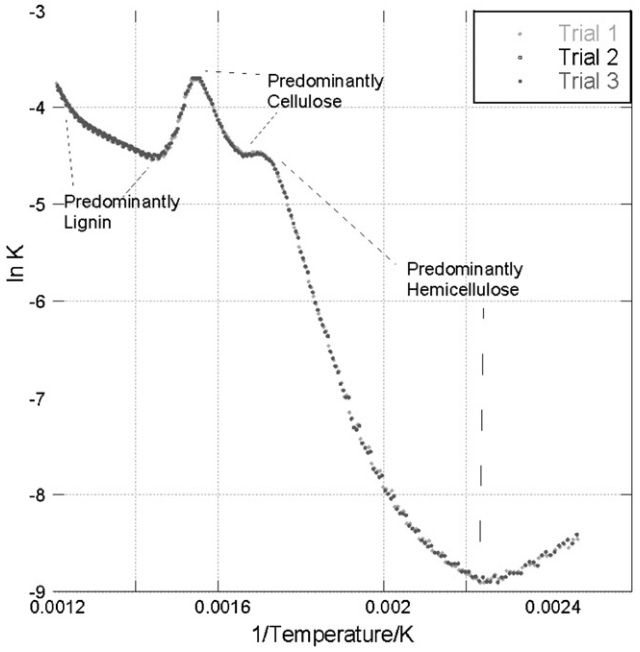

Fig. 3. Arrhenius plot for palm trunk, 125–250 μm fraction, heated at 100 °C min^{-1}.

wide range of 160–900 °C. In Table 1 and S1–S8 the data are divided into three sets, one each for the low-temperature (between 160 and 310 °C), mid-temperature (320–380 °C), and high-temperature (400–560 °C) mass loss regimes. As we see in Table 2, the average values for each mass fraction for each material (leaf, stalk, trunk) at each fraction and ramp rate, regardless of the material, size fraction, or ramp rate, are approximately 30% for the low-temperature region, 40–45% for the mid-temperature region, and 15–25% for the high temperature region. Of course, there is also a small amount of mass loss occurring at temperatures outside of these temperature ranges – especially with a higher ramp rate there may be small mass and heat transfer limitations. However, our data agrees quite well with literature findings on the relative amounts of hemicellulose, cellulose and lignin present in various biomass and the temperatures at which they decompose [13,14,20].

Fig. 3 shows the Arrhenius plot for the three runs of palm trunk, 125–250 μm fraction, heated at 100 °C min^{-1}. Besides the obvious reproducibility of the results, we see the three mass loss regimes corresponding roughly to the loss of predominantly hemicellulose, cellulose and lignin, remembering that small amounts of material, especially lignin, are found to decompose throughout the entire experiment. As done by Grammelis and co-workers [25] for paper biomass, we determined the activation energy and pre-exponential factor of the palm biomass by splitting the $\ln(k)$ vs. $1/T$ plot into three different fractions. As often noted in the literature, considering the devolatilization of biomass as a combination of the pyrolysis of three segments: cellulose, hemicellulose, and lignin, fits the palm pyrolysis data quite well, illustrated in Fig. 3 [26]. The activation energies of the low-temperature mass fraction (predominantly hemicellulose) range from approximately 60 to 120 kJ mol^{-1} depending on the plant material and temperature ramp rate; the highest activation energy in the 160–310 °C temperature range was seen for the 300–500 μm fraction of palm trunk pyrolyzed at 25 °C min^{-1} (~117 kJ mol^{-1}), and the lowest for the three palm leaf fractions pyrolyzed at 100 °C min^{-1} (~64 kJ mol^{-1}). For the mid-temperature (predominantly cellulose) range, the highest activation energy occurred for the two smallest palm stalk fractions pyrolyzed at 25 °C min^{-1} (~155 kJ mol^{-1}), and the lowest for the two smallest palm leaf fractions pyrolyzed at 100 °C min^{-1} (~69 kJ mol^{-1}). Conversely, for the predominantly lignin portion (high-temperature mass loss regime) we see the highest activation energy for the palm stalk pyrolyzed at 100 °C min^{-1} (23–26 kJ mol^{-1}) and the lowest for the smallest palm trunk particles pyrolyzed at 25 °C min^{-1} (~17 kJ mol^{-1}). These values agree well with activation energies for other biomass in the literature.

In a study on the pyrolysis of Malaysian oil palm biomass, Idris et al. [15] find activation energies for palm mesocarp fiber of 166 and 216 kJ mol^{-1} for two mass fractions (they do not report a third) and for palm kernel shell from 170 to 192 kJ mol^{-1} for the two mass fractions. It is not clear at what isothermal temperature these experiments were run. Using a heating rate of 20 °C min^{-1}, Pantoleontos et al. [27] determine kinetic constants for various solid waste samples. They find activation energies for forest residue of 118.0, 198.7, 104.7 and 86.6 kJ mol^{-1} for the first through fourth fractions, respectively (some biomass samples show a fourth separate peak on the Arrhenius diagram, often attributed to further decomposition of lignin). For meat and bone meal, Pantoleontos et al. report E_as of 66.9, 132.9, 199.7, and 77.6 kJ mol^{-1} for the four mass fractions at increasing temperature ranges, respectively. Finally, this group reports the activation energies of residue-derived fuel (RDF) for a first fraction of 113.0 kJ mol^{-1}, then third as 206.2, fourth as 36.8, and last as 34.0 kJ mol^{-1}. The temperature range for the "second" mass loss regime of the other samples was not consistent with the RDF. In another example [25], Grammelis et al., investigating the pyrolysis behavior of waste paper materials (magazine paper, cardboard, newsprint, copy paper, recycling paper) find activation energies for the first mass fraction ranging from 107 to 137 kJ mol^{-1}, for the second fraction from 199 to 232 kJ mol^{-1}, and for the third fraction from 30 to 48 kJ mol^{-1}. As can be seen, the activation energies determined in this study for the pyrolysis of cabbage palm are well within ranges for other biomass samples as determined by other researchers.

A distinct trend emerges when we look at the global average data, seen in Tables 2 and 3. Specifically, the particle fraction has very little effect on the onset/endset temperatures of each mass loss regime, the activation energy, pre-exponential factor or mass loss fraction. The differences across fractions are almost all within ± one standard deviation of the three trials for each fraction. Indeed, if we combine the data for the three fractions, as we see in Table 3, the values of all three fractions across the nine trials for each material and ramp rate are so close that the standard deviation actually shrinks across the data sets. More importantly though is the observed impact of temperature ramp rate on the activation energy and pre-exponential factor, seen clearly in Table 3.

For the low-temperature and mid-temperature mass loss fractions (corresponding largely to hemicellulose and cellulose) we see that as the temperature ramp rate increases from 25 to 50 to 100 °C min^{-1} the activation energy decreases. That is, the activation energy of the 25 °C min^{-1} ramp rate for each palm material is higher than that of the 50 and 100 °C min^{-1} ramps. Interestingly, for the high-temperature mass loss fraction, corresponding to mostly decomposition of lignin, the activation at 25 °C min^{-1} is lower than the activation energies of the 50 and 100 °C min^{-1} ramp rates.

A thermal gradient likely exists from the surface of the particle to the core, which means that at higher heating rates there is potentially a larger lag in heating [19,20]. This lag is observed in Figs. 4–6 in terms of activation energy. During pyrolysis, the solid fuel undergoes a series of changes, beginning with heat transfer from the heat source to increase the fuel temperature. Primary pyrolysis reactions release volatiles and form a carbonaceous char. These volatiles transfer into the cooler solid regions of the unpyrolyzed fuel, potentially limited by both heat and mass transfer. Furthermore, a portion of the volatiles may condense in the cooler parts of the fuel, initiating secondary reactions that form tar, occurring simultaneously with the primary reactions. Finally, the solid

Table 3
Global averages of palm stalk, leaf and trunk pyrolyzed at 25, 50, 100 °C min^{-1}, all size fractions averaged together (standard deviation reported for three values for each of three fractions) including overall heat of pyrolysis of each material across temperature range as determined by DSC.

	Low temperature mass loss regime					Mid temperature mass loss regime				
	Onset T (K)	Endset T (K)	E_a (kJ mol^{-1})	A ($s^{(-1)}$)	Mass loss fraction	Onset T (K)	Endset T (K)	E_a (kJ mol^{-1})	A ($s^{(-1)}$)	Mass loss fraction
Palm stalk 25 °C min^{-1}	446.0 ± 2.1	556.7 ± 0.8	88.5 ± 0.6	1.58E+06 ± 2.0E+05	0.30 ± 0.005	587.4 ± 1.2	619.3 ± 0.3	152.1 ± 6.8	4.61E+11 ± 3.6E+11	0.44 ± 0.01
Palm stalk 50 °C min^{-1}	429.2 ± 1.1	565.7 ± 1.6	78.1 ± 0.2	1.06E+05 ± 9.6E+03	0.29 ± 0.009	595.5 ± 1.4	628.1 ± 0.6	134.6 ± 3.2	7.07E+09 ± 4.0E+09	0.45 ± 0.01
Palm stalk 100 °C min^{-1}	438.1 ± 4.0	572.7 ± 3.7	79.9 ± 3.0	1.86E+05 ± 1.5E+05	0.28 ± 0.008	596.3 ± 2.4	637.9 ± 1.8	101.3 ± 2.5	7.63E+06 ± 3.1E+06	0.44 ± 0.01
Palm leaf 25 °C min^{-1}	447.8 ± 5.0	555.0 ± 0.7	78.1 ± 0.2	1.38E+05 ± 6.9E+03	0.28 ± 0.000	590.2 ± 1.4	621.8 ± 0.3	134.9 ± 7.3	1.15E+10 ± 1.0E+10	0.38 ± 0.01
Palm leaf 50 °C min^{-1}	427.0 ± 2.9	563.9 ± 1.3	69.5 ± 0.1	1.54E+04 ± 1.2E+02	0.27 ± 0.007	596.5 ± 0.7	631.2 ± 0.8	112.7 ± 5.5	9.07E+07 ± 8.3E+07	0.38 ± 0.02
Palm leaf 100 °C min^{-1}	441.1 ± 2.2	571.4 ± 0.9	64.3 ± 0.3	4.30E+03 ± 3.9E+02	0.27 ± 0.005	593.1 ± 1.0	638.0 ± 1.4	66.7 ± 3.6	7.03E+03 ± 3.9E+03	0.39 ± 0.02
Palm trunk 25 °C min^{-1}	458.8 ± 4.7	553.0 ± 1.2	115.7 ± 1.5	9.34E+08 ± 3.3E+08	0.28 ± 0.01	589.3 ± 1.0	621.9 ± 1.6	142.3 ± 4.4	4.29E+10 ± 2.9E+10	0.44 ± 0.02
Palm trunk 50 °C min^{-1}	436.6 ± 7.3	561.2 ± 2.8	97.6 ± 5.0	1.52E+07 ± 1.8E+07	0.29 ± 0.005	597.7 ± 0.6	630.7 ± 0.4	124.2 ± 8.0	1.26E+09 ± 1.2E+09	0.43 ± 0.04
Palm trunk 100 °C min^{-1}	446.3 ± 0.8	575.5 ± 2.7	84.4 ± 3.1	3.91E+05 ± 2.2E+05	0.27 ± 0.009	601.4 ± 3.9	640.5 ± 3.5	83.5 ± 6.7	3.18E+05 ± 2.5E+05	0.44 ± 0.01

	High temperature mass loss regime					All temperatures
	Onset T (K)	Endset T (K)	E_a (kJ mol^{-1})	A (s^{-1})	Mass loss fraction	Heat of pyrolysis (J g^{-1})
Palm stalk 25 °C min^{-1}	661.3 ± 3.4	834.3 ± 5.4	21.9 ± 0.2	0.48 ± 0.02	0.17 ± 0.002	5620 ± 653
Palm stalk 50 °C min^{-1}	677.1 ± 2.1	825.6 ± 3.8	24.8 ± 0.9	0.75 ± 0.11	0.16 ± 0.006	4066 ± 618
Palm stalk 100 °C min^{-1}	688.8 ± 9.1	826.2 ± 7.3	24.4 ± 1.9	0.75 ± 0.29	0.18 ± 0.003	2059 ± 267
Palm leaf 25 °C min^{-1}	658.1 ± 6.5	821.3 ± 2.9	19.3 ± 0.4	0.33 ± 0.02	0.22 ± 0.002	7331 ± 954
Palm leaf 50 °C min^{-1}	663.7 ± 0.4	814.5 ± 7.6	20.7 ± 0.4	0.41 ± 0.01	0.15 ± 0.005	4087 ± 423
Palm leaf 100 °C min^{-1}	667.7 ± 1.6	728.2 ± 0.8	23.2 ± 0.4	0.55 ± 0.03	0.23 ± 0.004	3345 ± 315
Palm trunk 25 °C min^{-1}	675.5 ± 3.6	830.7 ± 10.3	18.7 ± 1.7	0.28 ± 0.08	0.18 ± 0.008	7659 ± 746
Palm trunk 50 °C min^{-1}	685.9 ± 3.0	826.8 ± 4.5	20.7 ± 0.9	0.36 ± 0.05	0.17 ± 0.007	5188 ± 758
Palm trunk 100 °C min^{-1}	691.3 ± 6.6	818.4 ± 3.9	19.9 ± 1.6	0.34 ± 0.08	0.18 ± 0.004	5583 ± 807

Fig. 4. Activation energy versus temperature ramp rate for low temperature mass loss range (predominantly hemicellulose) (•), mid temperature mass loss range (predominantly cellulose) (■) and high temperature mass loss range (predominantly lignin) (◆) of palm leaf, all size fractions averaged.

further decomposes, and at longer residence times and higher temperature and pressure profiles other reactions such as water–gas shift reactions, radical recombination, and dehydrations may also occur [11]. We are well below the temperature and residence time for which these further reactions occur (as noted by the constant mass plateau observed at 600 °C).

Figs. 4–6 show the activation energy versus temperature ramp rates for the palm leaf, stalk, and trunk, respectively, for each temperature mass loss range. For all three materials, the highest

Fig. 5. Activation energy versus temperature ramp rate for low temperature mass loss range (predominantly hemicellulose) (•), mid temperature mass loss range (predominantly cellulose) (■) and high temperature mass loss range (predominantly lignin) (◆) of palm stalk, all size fractions averaged.

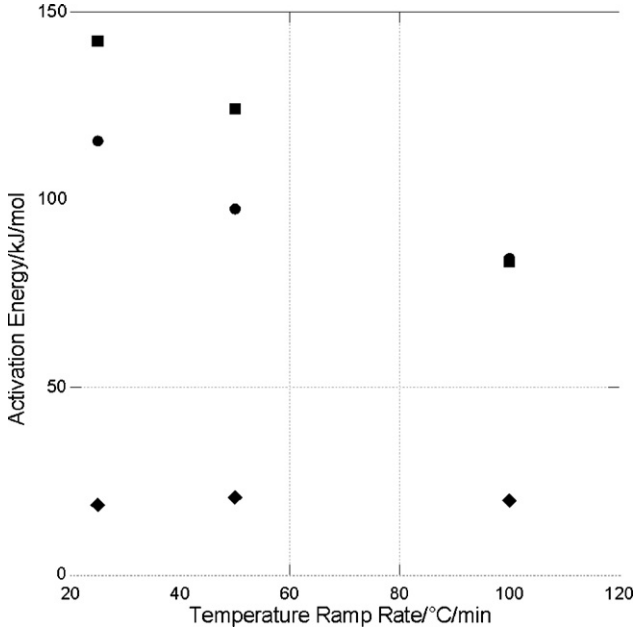

Fig. 6. Activation energy versus temperature ramp rate for low temperature mass loss range (predominantly hemicellulose) (●), mid temperature mass loss range (predominantly cellulose) (■) and high temperature mass loss range (predominantly lignin) (◆) of palm trunk, all size fractions averaged.

activation energies are seen for the mid-temperature mass loss fraction. In other words, the decomposition of the primarily cellulose fraction has a higher energy penalty than the decomposition of the predominantly hemicellulose or lignin fractions. The activation energy for the first two fractions decrease with increased heating rate, whereas for the high-temperature (mostly lignin) fraction, the activation energy actually increases slightly with heating rate.

These findings correspond well to the literature for other biomass sources. Dermirbas [28] finds a maximum pyrolysis oil yield and minimum char yield of beech trunk barks at 425 °C at a heating rate of 100 °C s^{-1}, as compared to 2, 5, 10, 20, and 40 °C s^{-1}. Likewise, Putan et al. found that for the pyrolysis of cotton stalk under a slow heating rate of 5 °C min^{-1}, each particle has time to reach the pyrolytic temperature range (as noted by the formation of reaction products), but that the oil yield was maximized at the highest heating rate of 550 °C min^{-1}. They note that particle size has little impact on pyrolysis products and kinetics. We also see a consequence of slower heating rate on the enthalpy of pyrolysis measured via the differential scanning calorimeter in tandem with the TGA measurements. As Table 3 shows, the heat requirement to evolve these pyrolytic gases is substantially higher at lower temperature rates.

In an investigation into the pyrolysis of sesame stalk, Ates et al. probe the effect of temperature, particle size (0.224–1.8 mm), heating rate (100–500 °C min^{-1}), and nitrogen flow rate (70–800 cm^3 min^{-1}). Bio-oil yields were not dependent on the particle size, though the maximum oil yield was dependent on the other variables (maximum occurred at 550 °C, heating rate of 500 °C min^{-1}, and N_2 flow rate 200 cm^3 min^{-1}) [29]. While we did not investigate the bio-oil yield, our findings in terms of activation energy being lower for higher temperature ramp rates may indeed correlate to the improved bio-oil yields seen at higher temperature ramp rates. At higher ramp rates – and lower activation energies – we are likely seeing less secondary reactions occurring among volatile compounds and solid fuel, thus correlating with increased bio-oil yield.

The pyrolytic process is the combination of multiple heterogeneous chemical reactions. A general consensus exists for an overall biomass pyrolysis scheme, whereby free moisture of the solid evaporates, followed by unstable polymer degradation. As temperature increases the more stable components begin to decompose, releasing volatiles from the solid matrix. A solid char residue forms during primary decomposition (between 200 and 400 °C) and undergoes subsequent aromatization at temperatures above 400 °C [30]. Though this reaction scheme is widely accepted, the understanding of what species transition in secondary reactions to form gases and tars is not well documented. Zhang et al. model pyrolysis as a series of reactions forming the gaseous products of CO, CO_2, CH_4, H_2 and H_2O. However, their own analysis of the gaseous products formed from pyrolyzing pinewood, red oak and sweet gum sawdust reveals these and at least twenty other organic compounds present in the gas phase alone, including ethane, acetylene, methanol, acetone and 2-butenal. While our and many others' overall kinetic studies of biomass reveal little influence of particle size on overall pyrolysis reaction rates, Zhang et al. [31] suggest that particle size alters the yields of H_2, CO and CH_4 as smaller particles with higher surface to volume ratios enables primary devolatilized products to more readily reach the vapor phase, minimizing secondary reactions. At lower heating rates the biomass particles are heated more gradually, leading to a more effective heat transfer and generally higher activation energy, which though it may decrease bio-oil yield, will also tend to decrease residue remaining after pyrolysis reactions [17].

4. Conclusion

The incorporation of renewable energy sources such as biomass into mainstream energy production depends on the development of a full understanding of the kinetics of biomass pyrolysis and decomposition reactions. As a readily available and simply cultivated fuel supply in the Southeastern United States, this investigation into the pyrolysis kinetics of cabbage palm shows its activation energies are comparable to other lignocellulosic biomass materials. The enthalpy of pyrolysis, as measured by differential scanning calorimetry, is substantially higher at lower temperature ramp rates – ranging from 2050 J g^{-1} for palm stalk at the higher heating rate to 7650 J g^{-1} at 25 °C min^{-1} for palm trunk. The activation energies of the palm trunk pyrolyzed at 100 °C min^{-1} are approximately 30% lower than those pyrolyzed at 25 °C min^{-1} for the low temperature fraction, 40% lower for the mid-temperature fraction, and 10% higher for the high temperature (mostly lignin) fraction. Similarly, the activation energy to pyrolyze palm leaf and stalk was 20% and 10% lower, respectively, for the high temperature mass loss fraction. For palm leaf, the mid-temperature mass loss regime had a 50% higher activation energy and the low-temperature a 20% higher activation energy to pyrolyze at 25 °C min^{-1} as opposed to 100 °C min^{-1}. Likewise, the activation energy of the low temperature mass loss fraction of palm stalk was 10% higher for 25 °C min^{-1} versus 100 °C min^{-1}, and 30% higher for the mid-temperature mass loss fraction. Overall we find that particle size fraction has little effect on the kinetics of cabbage palm pyrolysis, whereas the temperature ramp rate is critically important to the activation energy – and likely quality and quantity of bio-oil produced – for the thermochemical conversion of cabbage palm.

Acknowledgments

The authors thank Gary Kriner for harvesting the palm material used in this investigation. This material is based upon work supported by the National Science Foundation under grant no. NSF CBET-1127774.

Appendix A. Supplementary data

Supplementary data associated with this article can be found, in the online version, at doi:10.1016/j.jaap.2012.03.008.

References

[1] A.W. Meerow, Betrock's Guide to Landscape Palms, 8th ed., Betrock Information Systems, FL, 2002.
[2] Florida Department of Agriculture and Consumer Services, The Natural Role of Fire, Florida Forest Service, http://www.fl-dof.com/publications/fires_natural_role.html (accessed 3.09.11).
[3] W.G. Abrahamson, C.R. Abrahamson, Life in the slow lane: palmetto seedlings exhibit remarkable survival but slow growth in Florida's nutrient-poor uplands, Castanea 74 (2009) 123–132.
[4] K. McPherson, K. Williams, Establishment growth of cabbage palm, *Sabal palmetto* (Arecaceae), American Journal of Botany 83 (1996) 1766–1770.
[5] International Energy Agency, World Energy Outlook, Paris, 2008.
[6] H. Haykiri-Acma, S. Yaman, Effect of co-combustion on the burnout of lignite/biomass blends: a Turkish case study, Waste Management 28 (2008) 2077–2084.
[7] L. Ingram, D. Mohan, M. Bricka, P. Steele, D. Strobel, D. Crocker, B. Mitchell, J. Mohammad, K. Cantrell, C.U. Pittman Jr., Pyrolysis of wood and bark in an auger reactor: physical properties and chemical analysis of the produced bio-oils, Energy and Fuels 22 (2008) 614–625.
[8] Z. Luo, S. Wang, Y. Liao, K. Cen, Mechanism study of cellulose rapid pyrolysis, Industrial and Engineering Chemistry Research 43 (2004) 7607–7610.
[9] D.C. Elliott, Catalytic hydrothermal gasification of biomass, Biofuels, Bioproducts and Biorefining 2 (2008) 254–265, doi:10.1002/bbb.74.
[10] W. Mérida, P.-C. Maness, R.C. Brown, D.B. Levin, Enhanced hydrogen production from indirectly heated gasified biomass, and removal of carbon gas emissions using a novel biological gas reformer, International Journal of Hydrogen Energy 29 (2004) 283–290.
[11] D. Mohan, C.U. Pittman Jr., P.H. Steele, Pyrolysis of wood/biomass for bio-oil: a critical review, Energy and Fuels 20 (2006) 848–889.
[12] D. Vamvuka, E. Kakaras, E. Kastanaki, P. Grammelis, E. Kakaras, Pyrolysis characteristics and kinetics of biomass residue mixtures with lignite, Energy and Fuels 17 (2003) 740–778.
[13] A.E. Putun, N. Ozbay, E. Onal, E. Putun, Fixed-bed pyrolysis of cotton stalk for liquid and solid products, Fuel Processing Technology 86 (2007) 1207–1219.
[14] T. Mani, P. Murugan, N. Mahinpey, Pyrolysis of oat straw and the comparison of the product yield to wheat and flax straw pyrolysis, Energy and Fuels 25 (2011) 2803–2807.
[15] S.S. Idris, N.A. Rahman, K. Ismail, A.B. Alias, Z.A. Rashid, M.J. Aris, Investigation on thermochemical behaviour of low rank Malaysian coal, oil palm biomass and their blends during pyrolysis via thermogravimetric analysis (TGA), Bioresource Technology 101 (2010) 4584–4592.
[16] Şensöz, I. Demiral, H.F. Gerçel, Olive bagasse (*Olea europea* L.) pyrolysis, Bioresource Technology 97 (2006) 429–436.
[17] J.M. Encinar, F.J. Beltran, A. Ramiro, J.F. Gonzalez, A. Bernalte, Combustion kinetics of agricultural wastes, Journal of Chemical Technology and Biotechnology 64 (1997) 181–187.
[18] C. Di Blasi, Modeling chemical and physical processes of wood and biomass pyrolysis, Progress in Energy and Combustion Science 34 (2008) 47–90.
[19] M.J.J. Antal, G. Varhegyi, E. Jakab, Cellulose pyrolysis kinetics: the current state of knowledge, Industrial and Engineering Chemistry Research 37 (1998) 1267–1277.
[20] M. Van de Velden, J. Baeyens, A. Brems, R. Dewil, Fundamentals, kinetics and endothermicity of the biomass pyrolysis reaction, Renewable Energy 35 (2010) 232–242.
[21] J. Chattopadhyay, C. Kim, R. Kim, D. Pak, Thermogravimetric study on pyrolysis of biomass with Cu/Al_2O_3 catalysts, Journal of Industrial and Engineering Chemistry 15 (2008) 72–76.
[22] K. Celis, I. Van Driessche, R. Mouton, G. Vanhoyland, S. Host, Kinetics of consecutive reactions in the solid state: thermal decomposition of oxalates, Measurement Science Review 1 (2001) 177–180.
[23] A. Saddawi, J.M. Jones, A. Williams, M.A. Wojtowicz, Kinetics of the thermal decomposition of biomass, Energy and Fuels 24 (2010) 1274–1282.
[24] H. Yang, R. Yan, H. Chen, D.H. Lee, C. Zheng, Characteristics of hemicellulose, cellulose and lignin pyrolysis, Fuel 86 (2007) 1781–1788.
[25] P. Grammelis, P. Basinas, A. Malliopoulou, G. Sakellaropoulos, Pyrolysis kinetics and combustion characteristics of waste recovered fuel, Fuel 88 (2009) 195–205.
[26] E. Ranzi, A. Cuoci, T. Faravelli, A. Frassoldati, G. Migliavacca, S. Pierucci, S. Sommariva, Chemical kinetics of biomass pyrolysis, Energy and Fuels 22 (2008) 4292–4300.
[27] G. Pantoleontos, P. Basinas, G. Skodras, P. Grammelis, J.D. Pinter, S. Topis, G.P. Sakellaropoulos, A global optimization study on the devolatilisation kinetics of coal, biomass and waste fuels, Fuel Processing Technology 90 (2009) 762–769.
[28] A. Demirbas, Determination of calorific values of bio-chars and pyrol-oils form pyrolysis of beech trunkbarks, Journal of Analytical and Applied Pyrolysis 72 (2004) 215–219.
[29] F. Ates, E. Putun, A.E. Putun, Fast pyrolysis of sesame stalk: yields and structural analysis of bio-oil, Journal of Analytical and Applied Pyrolysis 71 (2004) 779–790.
[30] T. Fisher, M. Hajaligol, B. Waymack, D. Kellogg, Pyrolysis behavior and kinetics of biomass derived materials, Journal of Analytical and Applied Pyrolysis 62 (2002) 331–349.
[31] J. Zhang, H. Toghiani, D. Mohan, C.U. Pittman Jr., R.K. Toghiani, Product analysis and thermodynamic simulations from the pyrolysis of several biomass feedstocks, Energy and Fuels 21 (2007) 2373–2385.